

a Mary Ann Liebert, Inc. DOI: 10.1089/3dp.2021.0242 Open camera or QR reader and scan code to access this article and other resources online.



# Iodine-Based Sensitization of Copper Alloys to Enable Self-Terminating Etching for Support Removal and Surface Improvements of Additively Manufactured Components

Sanaz Yazdanparast, Subbarao Raikar, Meredith Heilig, 2 and Owen J. Hildreth

#### **Abstract**

Advances in selective laser melting (SLM) of metals in the past two decades have made metals additive manufacturing more accessible for industrial adoption. Despite printing process improvements, postprocessing of SLM components has not improved much, resulting in considerable costs, delay, and design limitations. Building upon recent advances in sensitization-based self-terminating etching processes, this work details a new set iodine-based sensitization and etching chemistries that simplify the post-processing of copper (Cu) alloy components fabricated using SLM. This work demonstrates that iodine can be used to "sensitize" the surface of copper alloy components to form soluble copper iodide salt that can be then dissolved in common solvents, such as acetonitrile. This process removes a predefined amount of material from all interior and exterior surfaces in a self-terminating manner, enabling facile removal of internal and external supports, removal of any trapped powder, and the smoothing of interior and exterior surfaces. We demonstrate this process on GRCop (Cu-chromium-niobium) alloys due to their widespread use by the rocket propulsion industry along with a demonstration in copper (110) for applications in heat exchangers and electromagnetic transmitters/receivers. Our results provide the first systematic study on the effect of iodization temperature and duration on the thickness of the iodide region in GRCop-84 components. Additionally, the surface roughness before and after each iodization-dissolution was also quantified for GRCop-84 and showed 70% reduction in R<sub>a</sub> roughness from a high of 10 lm as-printed to a low of 3 lm after four iodization-dissolution cycles.

Keywords: GRCop, additive manufacturing, support removal, post-processing, roughness

#### Introduction

GRCop alloys (Copper [Cu]-chromium [Cr]-niobium [Nb]) comprise a set of advanced copper alloys with high temperature properties, such as excellent oxidation and creep resistance, high-elevated temperature strength, low thermal expansion, long low-cycle-fatigue lives, and good

thermal conductivity.<sup>1,2</sup> These properties make them attractive for use in rocket nozzles and as part of the combustion chamber liner for reusable launch vehicles. Two main GRCop alloys are GRCop-84 (Cu-8 at.% Cr-4 at.% Nb) and GRCop-42 (Cu-4 at.% Cr-2 at.% Nb) containing highly stable Cr Nb precipitates as the strengthening phase of Cu matrix.<sup>3,42</sup>

Opposite page: A new set of iodine-based self-terminating etching processes have been developed that drastically simplifies post-processing, making it easy to remove support structures and surface roughness was reduced by at least 70%. As shown in this figure, the process removes supports and smooths surfaces in a geometry-agnostic manner. As a result, complex parts can be easily post-processed independent of geometric complexity. Image Credit: Subbarao Raikar.

<sup>&</sup>lt;sup>1</sup>Department of Mechanical Engineering, Colorado School of Mines, Golden, Colorado, USA.

<sup>&</sup>lt;sup>2</sup>AMPP Technologies, Lakewood, Colorado, USA.

The Cr<sub>2</sub>Nb phase also pins the grain boundaries, which refines and controls the copper grain size.<sup>5</sup> These alloys were originally developed in the 1990<sup>4</sup> for rocket propulsion applications and have only recently garnered broader industry interest because, while the material can be difficult to machine, it is relatively easy to form using selective laser melting (SLM) additive manufacturing (AM) techniques. Using SLM to fabricate GRCop components results in shorter lead times, lower costs, and increased complexity of GRCop components.<sup>6–8</sup>

SLM is not without its downsides. For example, the support structures used to reduce component distortion and to provide thermal pathways for heat dissipation<sup>9–11</sup> can be expensive to remove, increase lead times, and often require mechanical access, which limits design freedoms and increases build layout complexity.<sup>10–13</sup> In addition, reducing the as-built surface roughness while meeting geometric tolerances can be extremely difficult for components with complex geometries or inaccessible interior surfaces. This reduces fatigue performance<sup>14</sup> and, for rocket propulsion or heat exchanger components, reduced flow performance.<sup>15</sup> Either of which restricts the practical application of SLM.<sup>16</sup>

To address the above issues, Hildreth and colleagues have demonstrated a number of self-terminating etching processes for nickel, ferrous, and titanium-based alloys as an effective method to automate the post-processing of AMfabricated components. 17-19 In this method, the component is printed using standard equipment, materials, and recipes; then, after printing, the component is treated with a sensitizing agent to sensitize the top 100-200 lm of all interior and exterior surfaces (including all supports and trapped powder). The chemical stability of this "sensitized region" is designed to be significantly lower than the underlying component, allowing it to be selectively dissolved with a properly selected etchant. 17-19 Because only the sensitized region is dissolved, the process is inherently selfterminating—making it able to remove internal and external support structures, smoother internal and external surfaces, and remove trapped power while still maintaining overall component geometry.

This technique was originally developed for iron- and nickel-based alloys, such as stainless steel and Inconel, <sup>18,19</sup> that derive their corrosion resistance from high concentrations of passivating elements. Carbon was used as the sensitizing agent for these materials because it reacts with and captures the passivating elements, such as Cr, by forming carbide precipitates. <sup>18–21</sup> When enough passivating elements are captured, the surface no longer self-passivates and becomes "sensitive" to corrosion. Since the supports and trapped powder are relatively thin, they end up completely sensitized along with many of the surface defects that increase surface roughness. After sensitization, the sample is electrochemically etched under a bias that anodically etches the sensitized region while cathodically protecting the underlying, unsensitized component material.

Carbon-based sensitization does not work for every metal alloy. For example, titanium does not form low temperature carbides and, even if it did, titanium itself is self-passivating and would not see an exploitable drop in corrosion resistance. To address this issue, Hildreth and others recently demonstrated a modified sensitization approach that uses sulfur to transform the surface of SLM-processed Ti-6Al-4V (Ti64)

components.<sup>17</sup> The sulfur reacts with the titanium, aluminum, and vanadium to form soluble sulfides that can be selectively dissolved using a mixture of sulfuric acid with an oxidizing agent acting as a corrosion inhibitor that protects the underlying Ti64 component material.

Because the sulfidation of titanium alloys is driven by the transport of metal outward through the sulfide film instead of sulfur being driven into the metal, the metal/sulfide interface is extremely "sharp" and the sulfide film can be completely removed without sulfur contaminating the underlying metal. Additionally, since the diffusion rate of the metal outward decreases with increasing sulfide film thickness, the sensitization process itself is effectively self-limiting even for components with complex geometries. Overall, this process is reasonably fast and simplifies post-processing of Ti64 components.

Building off the sulfur-based sensitization approach used for Ti64, our group initially attempted to use sulfur as a sensitizing agent for copper alloys. Unfortunately, the process was more complicated than desired. While copper does form soluble sulfides, removing those sulfides chemically or electrochemically without unwanted damage or morphology changes to the underlying component material proved to be challenging. Copper does not form stable, passivating oxides the way titanium alloys do, and the electrochemical biases needed to protect the underlying copper often resulted in copper ions from the dissolved copper sulfides being reduced and deposited back onto the component. While some workarounds were developed, the processing window was determined to be too narrow for practical use and alternative chemistries were tested.

Addressing the above issues, this article introduces iodine as a sensitizing agent for copper alloys as an effective alternative to carbon- and sulfur-based sensitization approaches. The self-terminating etching process in copper alloy components is schematically illustrated in Figure 1. Components are first printed using existing SLM parameters, materials, and support design strategies. Next, the component with supports is placed in a heated furnace containing iodine vapor. The iodine reacts with the copper to form soluble iodides that are easily dissolved without impacting any underlying unsensitized material. Each cycle removes \*30–601m of material (depending on processing conditions) and can repeated as many times as necessary to remove the overall targeted amount of material from the component's surfaces and supports.

Like the sulfur-based approach used for Ti64, this new iodine-based chemistry also shows an extremely sharp interface between the sensitized region and the underlying component material with no residual sensitizing agent left in the component surface after etching. Additionally, the process works relatively at low temperatures (100–250°C) and does not initiate microstructure evolution. More importantly, iodine readily forms metal halide salts that, due to the increased ionic character of these bonds, are readily dissolved in common solvents that are chemically compatible with the underlying metal alloy. For example, acetonitrile was used to dissolve the copper iodide within the iodine sensitize region. This mild solvent does not react at all with the underlying GRCop alloys and enables this process to be self-terminating, geometry agnostic, and easy to implement.

# **Iodine-based Self-Terminating Etching**

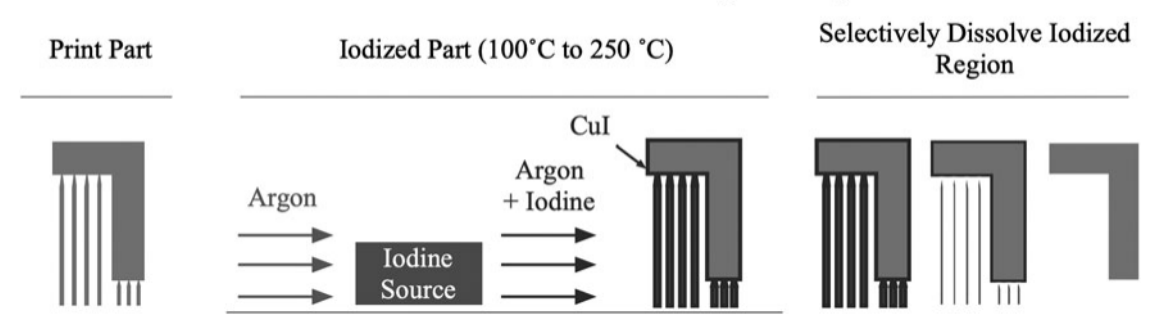


FIG. 1. Schematic illustration of the iodine-based sensitization and etching of copper alloys. The components are iodized in a furnace. The outer surface of the components (30–60 lm) reacts with iodine forming CuI that is readily removed by dissolving this sensitized region in acetonitrile. The net result is a facile method to post-process copper components. CuI, copper(I) iodide.

For this work, the effect of temperature and duration of the iodization process was systematically studied on GRCop-84 (Cu-8Cr-4V) alloy. In addition, we report the GRCops support consumption thickness as a function of iodization–dissolution cycle and verify that the iodides are fully removed using X-ray diffraction (XRD) and energy dispersive X-ray spectroscopy. The surface roughness as a function of sensitization and etch cycle is reported and shows 70% reduction in roughness. The overall process was demonstrated on both Cu (110) and GRCop-42 components with complex geometries to show that the process can remove support structures while improving surface finish.

Overall, this article continues the evolution of self-terminating etching for metals alloys. Originally starting with carbon-based sensation for stainless steel, then sulfur-based sensitization that works in titanium alloys, and now iodine-based sensitization of copper alloys. While this article discusses our results on copper alloys, future work will continue to explore the utility of using halides to create self-terminating etching processes for other material systems.

# Materials and Methods

#### Sample preparation

GRCop-84 disks (15 mm diameter, 3.5 mm thick) and GRCop-42 cubic samples (10 · 10 · 4 mm, length · width height) built on top of 10 mm tall supports were printed by external vendors (Quadrus and Elementum 3D) using their Concept Laser M2 and EOS M290 printers, respectively. The disks were printed with the circular faces parallel to the printer bed (perpendicular to the build direction). The chemical compositions of the GRCop-84 and GRCop-42 powders for printing samples as supplied by the vendors are listed in Supplementary Table S1. The print settings were not supplied by the vendors and was not considered critical to the experiment itself since the samples were reasonably dense with minimal surface porosity (reasonable was qualitatively determined as not seen many pores near surfaces as observed in optical microscope images of cross-sectional samples) that would impact iodization kinetics (surface pores would have different metal and iodine diffusion rates vs. bulk material).

To perform consistent roughness measurements in different orientations of the disks before and after selfterminating etching process, small cuts were made into edge of the disk parallel to the sample build direction using a metal file. These cuts were only used for identification purposes and are not expected to impact the sensitization or etching process. These samples were then cleaned in an ultrasonic bath with deionized (DI) water, followed by isopropyl alcohol (IPA) for 5 min and then dried with compress N<sub>2</sub> before iodization. A smooth surface was needed to study the effect of temperature and time on the iodization process of GRCop alloy. For these samples, one side of the GRCop-84 disks was ground with silicon carbide papers of 320, 400, and 600 grit and then cleaned with DI water, followed by methanol, acetone, and IPA. The samples were dried with compressed N<sub>2</sub> gas to remove any excessive alcohol on the surface of the disks.

The support removal study was carried out on rectangle, spiral, frog, Mobius shape, and the captured sphere parts with support structure fabricated from copper and heattreated GRCop-42. These samples were cleaned with DI water, IPA, and then dried with compressed N<sub>2</sub>. The GRCop samples required a heat treatment before sensitization to properly precipitate the CrNb precipitates. We found that performing heat treatment results in a cleaner surface with little to no residual Cr oxides. We followed the standard heat treatment procedure for SLM GRCop components. Heat treatment was performed in a tube furnace (Lindberg HT55342C) under Ar flow at 0.45 standard liters per minute (SPLM) with 5-h ramp to 900°C, followed by a 5 h holding period at this temperature and then furnaced cooled to room temperature.

#### Iodization of GRCop alloys

Iodization of GRCop-84 disks was performed in the tube furnace. The disks were loaded in an alumina boat and placed in the center of the furnace with the ground side facing the carrier gas. After loading the samples, the tube was purged with the purified Ar for 2h at 0.45 SPLM to remove any trapped air from the tube. The iodine powder (‡99.99% METALS BASIS; Sigma–Aldrich) was placed inside a flask connected to the tube and was heated between 35°C and 40°C

to vaporize some of the iodine. After purging with Ar gas for 2 h, the furnace was heated to the temperatures in the range of 150250°C at 10°C/min.

After reaching the target iodization temperature, vaporphase elemental iodine was carried by Ar to the tube furnace and the samples were iodized from 15 to 360 min. Next, the samples were either furnace cooled or air cooled. Furnace cooling was conducted to study the effect of temperature and insured that minimal oxygen would be present to contaminate the samples (typical oxygen levels of our furnace were measured at <2 ppm). Air cooling was performed to study the effect of iodization time since this study is more time-sensitive and air cooling would provide a faster cooling rate and a better "square wave" type temperature function.

Due to size limitations of the tube furnace, parts with support structures were iodized using a simpler setup that allowed for larger parts, but less control over temperature. For these samples, iodization was performed by placing the samples and iodine powder in a sealed gas jar under N<sub>2</sub> and then heated between 150°C and 170°C. The first samples (a spiral and a frog) were iodized overnight for \*15 h. This was arbitrarily chosen to ensure that full iodization of the supports is achieved. The second set of samples (Mobius shape and the captured sphere) were iodized between 1 and 4 h to roughly see how much time was needed for a reasonable sensitization depth. Future work will examine the reaction and mass transport kinetics of this process so that iodization times can be intelligently selected.

#### Dissolution of iodized layer

Most of the iodized samples were etched using room temperature acetonitrile (>99.9%; Fisher Chemical) with magnetic stirring for 1 h, followed by sonication for 10 and 30 min. The Mobius shape and the captured sphere samples were sonicated for just 5 min in DI water and 10 min in acetonitrile to roughly see how quickly this step could be. Just as with the iodization step, future work will examine the dissolution rates of the halide salts so that the etching conditions can be intelligently selected. After sonication, all samples were cleaned with DI water, then IPA, and dried by  $N_2$  gas.

#### Material characterization

For cross-sectional study of samples after iodization and dissolution processes, the samples were mounted in two steps. First, the disks were mounted with the iodized surface face up in a mixture of cold-curing epoxy (EpoFix; Struers) and nickel powder, Ni (200-mesh), inside 25.4 mm (1-inch) diameter mold cups. Then, the cured mounts were cross-sectioned using a metallographic saw (LECO MSX-250 M2) with an  $Al_2O_3$  abrasive blade. The resultant samples with the cut face down were mounted in the same mixture as mentioned above in larger mold cups (32 mm diameter). With this two-step mounting process, we were able to prevent the breaking of the fragile iodide layer from the GRCop during cutting.

The Ni powder was used to increase the conductivity of the mounted samples, especially the edge area for scanning electron microscopy (SEM) and energy dispersive spectroscopy (EDS). The mounted samples were ground with silicon

carbide papers ranging from 180 to 600 grit, followed by polishing with Microid diamond compound extender and 91m diamond suspension. Then, the samples were rinsed with DI water and dried using  $N_2$  gas.

XRD patterns of the heat-treated GRCop-84 disks before iodization, after iodization, and after dissolution of the iodide layer were collected by Bruker D2 PHASER system using Co-K<sub>a</sub> radiation (wavelength 1.789 Å). To record the iodization-dissolution effect on the macroscopic scale of the samples, Nikon D3300 was used for digital photography. The morphology, cross-sectional study, and elemental compositions (line scans) of samples after iodization and dissolution were characterized by SEM (SEM, TESCAN MIRA3) equipped with Bruker XFlash 6j30 EDS. To examine the change of the thickness of the support during self-terminating etching process, light optical microscopy (Zeiss Axio Vert.A1) was used. Before iodization and after each cycle of iodization-dissolution, mass and dimensions of the samples were measured by XS105 Mettler Toledo mass balance and handheld Fowler calipers.

The surface roughness measurements were conducted using a Bruker DektakXT contact profilometer using a 2 lm stylus tip radius with 5.6 mm scan lengths at 1200 lm/min. The scans were at the center on the flat surface of the disks and 1 mm on both the sides of the center (the inset in Fig. 6). The  $R_a$  roughness was calculated based on ISO 4287 standard with a long cutoff wavelength  $(k_{\rm c})$  of 0.8 mm and a short cutoff wavelength  $(k_{\rm s})$  of 2.5 lm.  $^{22}$ 

### Results and Discussion

XRD patterns of heat-treated GRCop-84 disks before iodization, after iodization, and after etching are shown in Figure 2. The heat-treated sample before iodization contains copper as the primary phase with low intensity of other phases that can be attributed to cuprous oxide, niobium(II) oxide, and Cr. After iodization, high intense peaks of

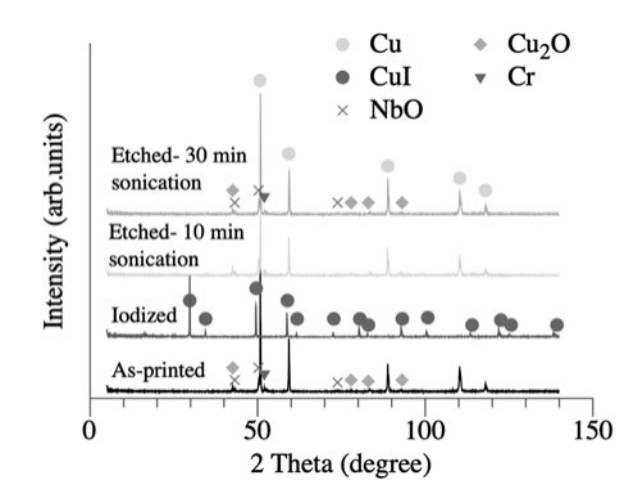


FIG. 2. XRD (CoK<sub>a</sub>) patterns of heat-treated GRCop before iodization (black), after iodization at 200°C for 1 h (red), after etching with acetonitrile for 1 h, followed by sonication for 10 min (blue), and after etching with acetonitrile for 1 h with 30 min sonication (green). XRD, X-ray diffraction.

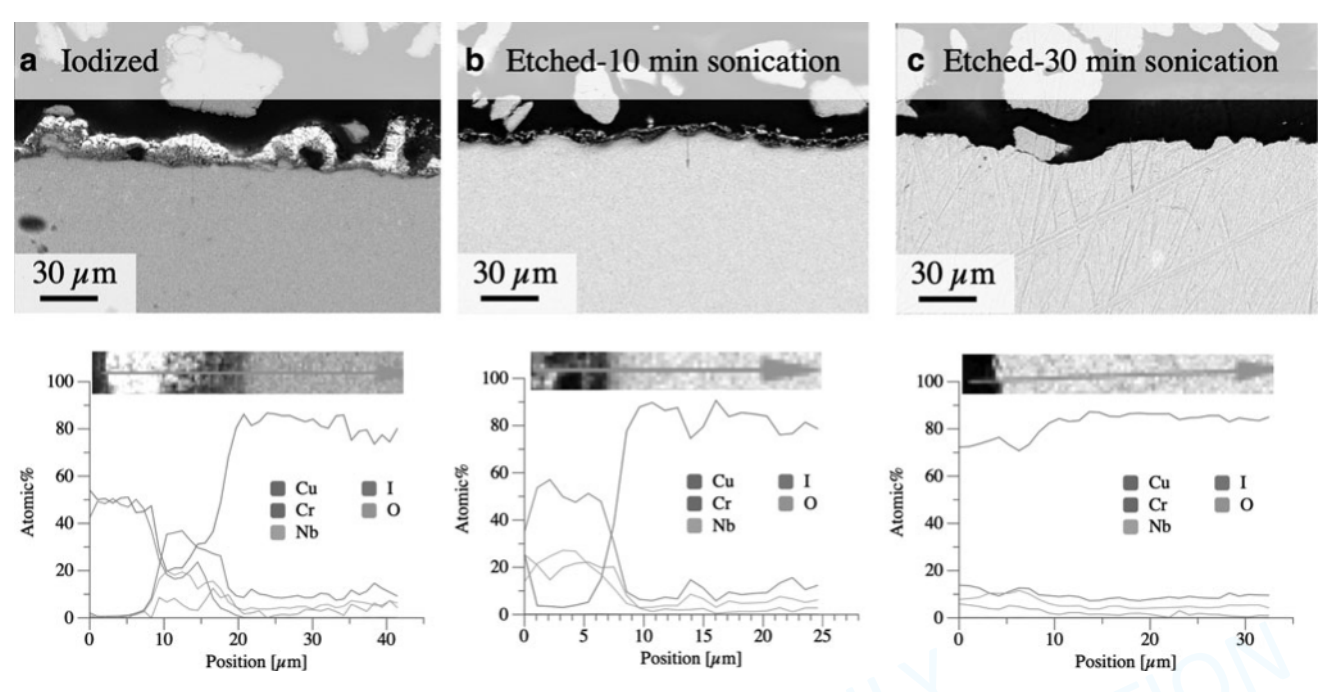


FIG. 3. EDS line scan result of heat-treated GRCop-84 (a) after iodization at 200°C for 15 min showing formation of CuI and oxide layer, (b) after etching with acetonitrile for 1 h followed by 10 min sonication, the CuI layer is removed while a thin inner layer mainly composed of Cr, Nb, and O elements is present, and (c) after etching with acetonitrile for 1 h followed by 30 min sonication, no trace of I and O is detected confirming the removal of the inner layer. EDS, energy dispersive spectroscopy; Cr, chromium; Nb, niobium.

copper(I) iodide (CuI) were observed, and after etching with acetonitrile, the XRD pattern is similar to the asprinted sample (before iodization), and mostly, copper phase has been detected showing that CuI was etched. However, the samples were darker in color possibly due to a layer of Nb and Cr oxides remaining on the surface (Supplementary Fig. S1). In Supplementary Figure S1, it is shown that the color of the disk after iodization—dissolution with 10 min sonication is darker than the disk with 30 min sonication.

To clarify the elemental composition of the etched surface, EDS line scans were performed both on the top surface (Supplementary Fig. S2b) and on the cross section of the samples (Fig. 3b, c). The EDS data in Supplementary Figure S2b show that the iodized region readily dissolves with a combination of acetonitrile and sonication. The cross-sectional EDS result in Figure 3b shows that the etched sample after sonication for 10 min contains a thin layer of Nb-and Cr-rich oxides remaining on the surface. These oxide particles are not well adhered to the surface and are easily removed after longer sonication (30 min) in acetonitrile as verified from the SEM (Supplementary Fig. S3d) and EDS data (Fig. 3c).

Supplementary Figure S3 and Figure 3 show the cross-sectional SEM images and the EDS line scan results of HT-GRCop-84 disk before and after iodization, and after iodization—etching processes. The printed surface of the HT-GRCop-84 disk is very rough, and its irregular surface is shown in Supplementary Figure S3a. After iodization at 200°C for 15 min, two nonuniform layers are formed (Supplementary Fig. S3b). The layers are classified as the outer (white color) and inner (gray color) layers. The EDS line scan

result (Fig. 3a) of the iodized sample shows that the outer layer is CuI, whereas the inner layer composed of Cr- and Nbrich oxides.

Formation of the Cr- and Nb-rich oxide layer in the iodized sample might be related to the leaks in the furnace and/or the decomposition of the iodides to oxides when exposed to moisture in the air or grinding/polishing. To study the effect of the moisture in the grinding/polishing on the CuI decomposition, the as-received CuI powder was stirred in both DI water and polishing liquid containing micron diamond compound extender and 9 lm diamond suspension for 2 h. Then, the powder was washed several times and dried in a vacuum desiccator. The XRD was performed on the resultant powder (Supplementary Fig. S4), and as it is shown in Supplementary Figure S4, no oxidation was observed in the CuI powder after treating with both DI water and polishing liquid.

This result confirms that the observed oxide layer in the iodized sample is not due to the decomposition of the CuI powder. To understand the effect of the atmosphere on the formation of the oxide layer during iodization process, we performed iodization on the capsulated sample. Supplementary Figure S5 shows the cross-sectional EDS line scan of the capsulated HT-GRCop-42 sample after iodization at 200°C for 120 min. It is shown that the oxygen level in the iodized layer is much lower compared with the GRCop sample that iodized in the Ar atmosphere inside the tube furnace (Fig. 3a). This result indicates that formation of the Cr- and Nb-rich oxide was due to the oxygen ingress leaks in the furnace.

After etching the iodized sample with acetonitrile and performing sonication for 10 min, the outer layer is

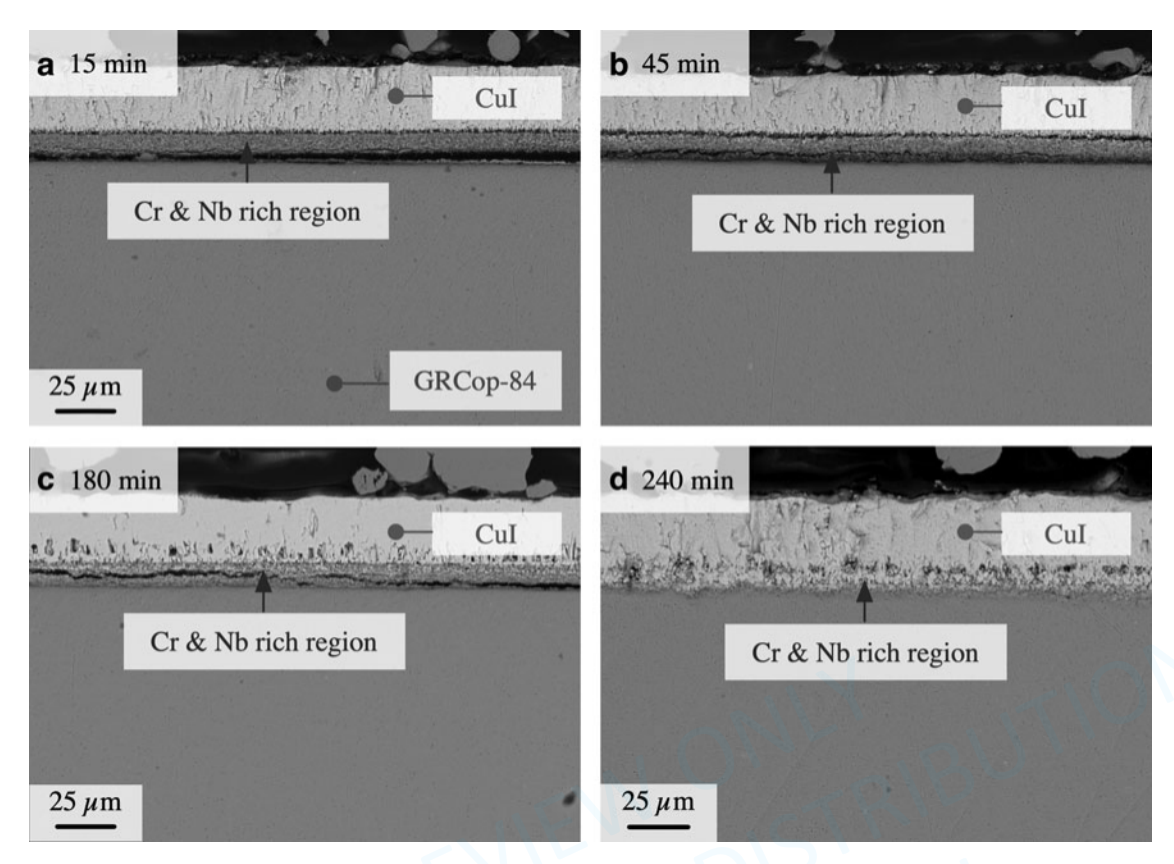


FIG. 4. Cross-sectional SEM images of the heat-treated GRCop-84 disks after iodization at 200°C for different times, (a) 15 min, (b) 45 min, (c) 180 min, and (d) 240 min, showing a slight increase of iodide layer thickness by increasing the time. Additionally, notice that the Cr- and Nb-rich regions start to diffuse into the CuI layer with increasing time. SEM, scanning electron microscopy.

completely removed, but the thin layer of the oxide particles is observed on the surface (Supplementary Fig. S3c). The absence of the iodine signal in the etched samples confirms that the iodides dissolve completely in the acetonitrile (Fig. 3b). The remained inner layer after etching is mainly composed of Cr, Nb, and O elements (Fig. 3b). After in-

creasing the sonication time to 30 min (Supplementary Fig. S3d), the whole oxide layer was completely dissolved in the acetonitrile, and no trace of oxygen was observed in the EDS result as shown in Figure 3c. This additional sonication time could be avoided if a fully sealed furnace is used during iodization.

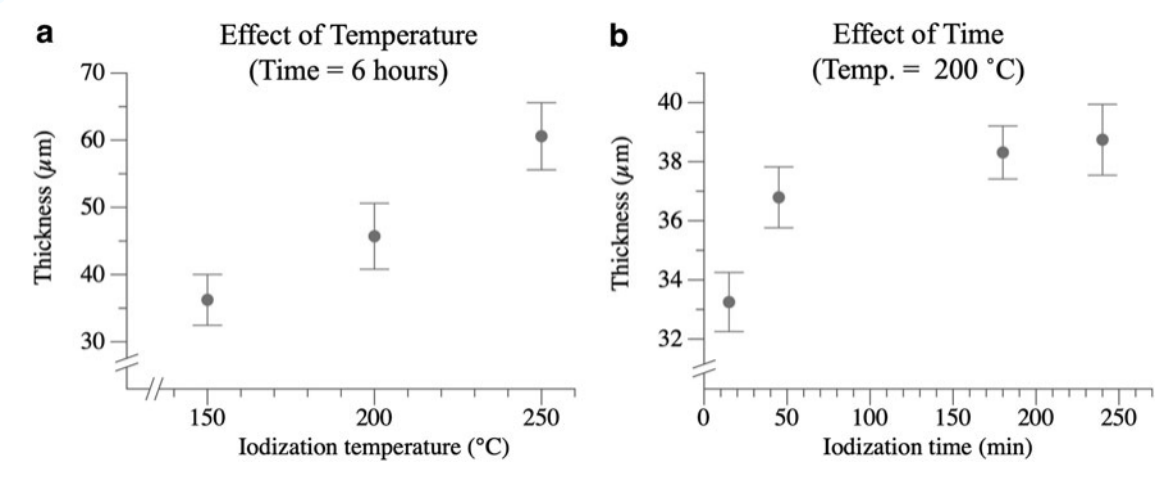


FIG. 5. Plots of (a) thickness versus iodization temperature for the GRCop-84 disks after iodization for 6 h and (b) thickness versus iodization time after iodization at 200°C, showing that the thickness of the iodide layer increases by increasing the iodization temperature and time. The effect of iodization temperature on the thickness of the films is more profound compared with the iodization time.

Supplementary Figure S6 (Supplementary Data) and Figure 4 show the cross-sectional SEM images of the heattreated GRCop-84 disks after iodization at different temperatures and time, respectively. Formation of a dense CuI layer with rough Cr- and Nb-rich regions at the GRCop/CuI interface is shown in all the iodized samples. From the SEM images, a sharp interface between GRCop and iodide layer is observed, suggesting that the diffusion kinetics of the iodization in GRCop is mostly due to the diffusion of metal into the iodide layer. The actual mechanisms and kinetics will be studied in the future. Measurements of the resultant layers after iodization process were performed using the ImageJ as shown in Figure 5. From Figure 5a, the thickness of the films increases by increasing the temperature from 150°C to 250°C by around 25 lm.

It is worth noting that the reported values for the thickness of iodized samples are the combination of both CuI and Crand Nb-rich regions. Comparing the cross-sectional SEM images in Supplementary Figure S6 shows that increasing the thickness of the films by increasing temperature is mostly due to the increasing of the CuI than the Cr- and Nb-rich layer. EDS data show that the Cr- and Nb-rich region will be oxide rich if the iodization environment contains oxygen greater than 15 ppm. Only Cr and Nb iodides were observed if the oxygen concentration in the iodization environment is less than 5 ppm. It has also been observed that iodide layer is fragile, and it has a high tendency for being peeled off and separate from GRCop base during sample preparation procedures as it shown clearly in Supplementary Figure S6c.

Figure 4 shows the cross-sectional images of the samples after iodization at 200°C for iodization durations from 15 to 240 min. From Figure 4a, the formation of the iodide layer is kinetically fast and a 33 lm iodide layer forms in only 15 min of iodization. Figure 5b shows the effect of iodization time on the resultant thickness. Increasing the time from 15 to 240 min only increases the iodide thickness by 5.5 lm. These results suggest that the temperature has a profound influence on the resultant iodide layer thickness compared with the iodization time. Comparing the cross-sectional SEM images

in Figure 4 shows that the iodization time affects the roughness of the resultant films at the interface region with GRCop-84 disks. By increasing the iodization time, the roughness at the interface of the film and GRCop disk increases as shown in Figure 4d.

To study the effect of self-terminating etching process on the surface roughness of the GRCop-84 disks, two types of surface roughness (Pa—arithmetic average of the unfiltered raw profile, and R<sub>a</sub>—arithmetic average of the roughness profile) were collected for the samples before iodization and after each iodization-dissolution cycle (Fig. 6). Surface roughness data were collected with three scans in three different directions: (1) parallel to the build, (2) perpendicular to the laser scan, and (3) 45° to the laser scan. In Figure 6a, it is shown that the P<sub>a</sub> roughness of the disk decreases by 70% from a high of 10 lm in as-printed disk to a low of 3 lm after four cycles of iodization-dissolution. After each cycle of iodization-dissolution, the surface roughness decreases and becomes more uniform, which is favorable for improving the fatigue strength and mechanical performance of the AM components. Although the value of Ra is slightly different from Pa roughness, similar behavior is observed for the Ra roughness as shown in Figure 6b.

The self-terminating etching process was also studied on different geometries of printed parts with support structures fabricated from GRCop-42 and copper (110). Initially, all the printed parts were iodized at 170°C for 15 h using a hot plate and air-cooled. Then, the iodized samples were etched with acetonitrile at 40°C with magnetic stirring for 1 h and sonicated for 30 min. During sonication, the acetonitrile color turned dark, and the solution was replaced until no color change was observed. Both iodization and etching were repeated for different cycles to completely remove the support structure from the printed parts. Supplementary Figure S7 shows the photos of HT-GRCop-42 rectangle after iodization and different iodization—etching cycles until the whole support was dissolved.

Figure 7 shows the optical microscopy images of the support structure at different cycles of iodization-dissolution. Reduction of the support thickness is clearly

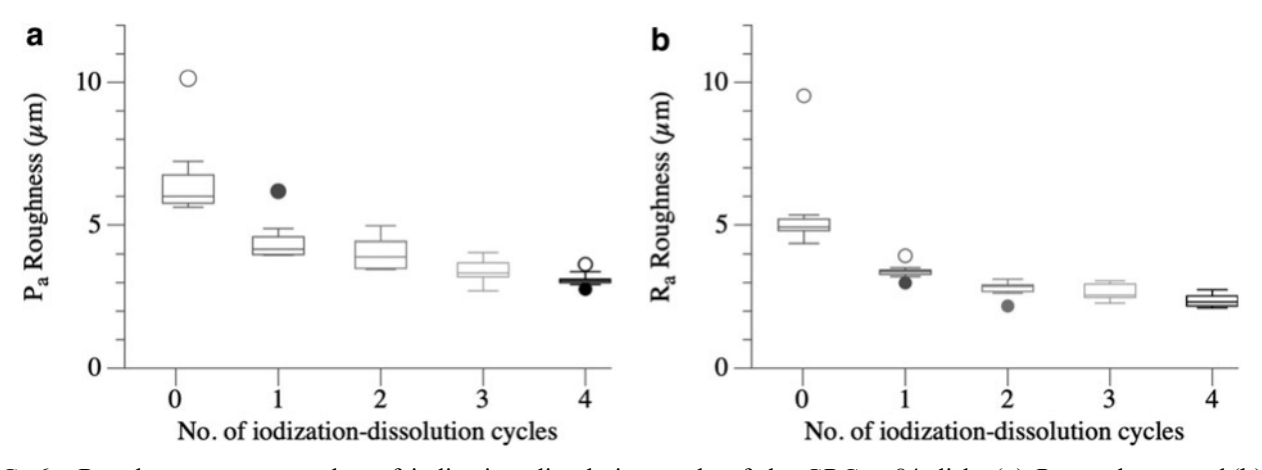


FIG. 6. Roughness versus number of iodization–dissolution cycle of the GRCop-84 disk. (a) P roughness and (b) R roughness, showing improvement of the surface roughness compared with the as-printed disk by self-terminating etching process.

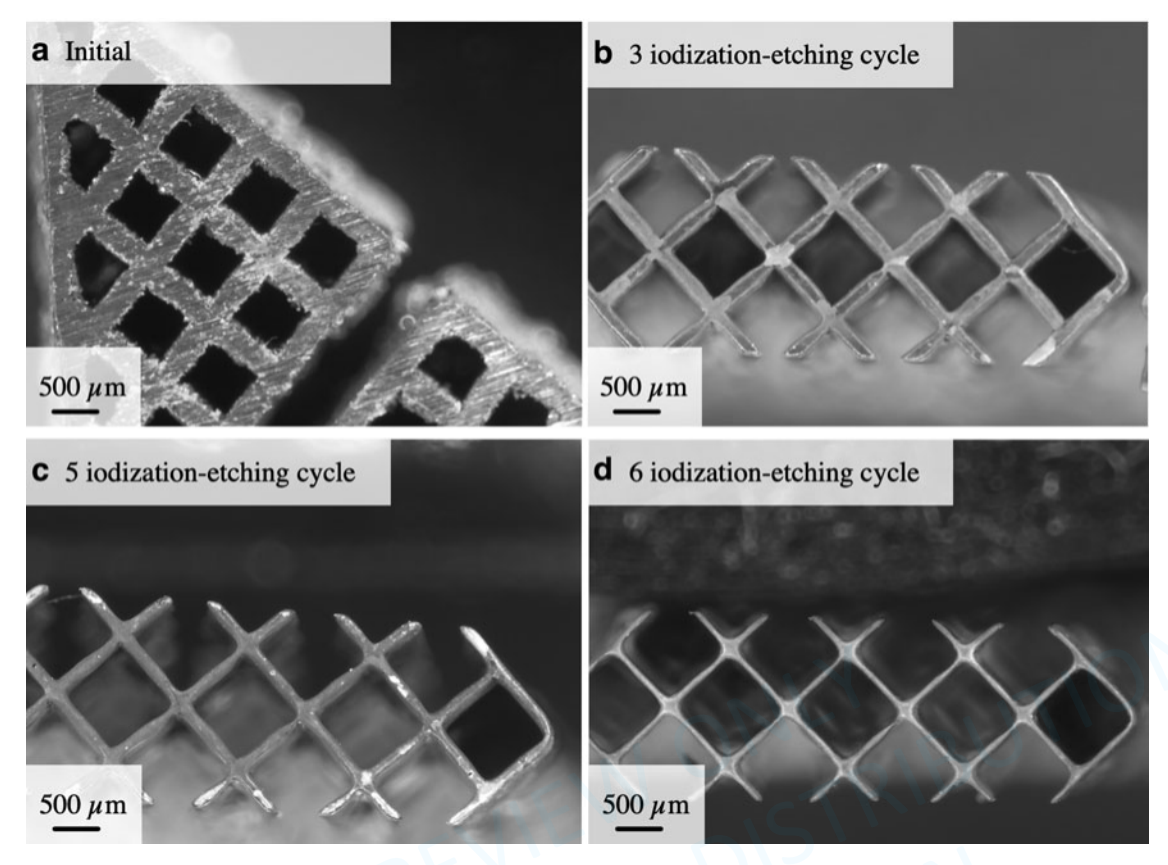


FIG. 7. Top-down optical microscopy images of the GRCop-42 with support structure. (a) Original sample, (b) three iodization–etching cycle, (c) five iodization–etching cycle, and (d) six iodization–etching cycle, showing thinning of the support structure after each cycle of iodization–etching process.

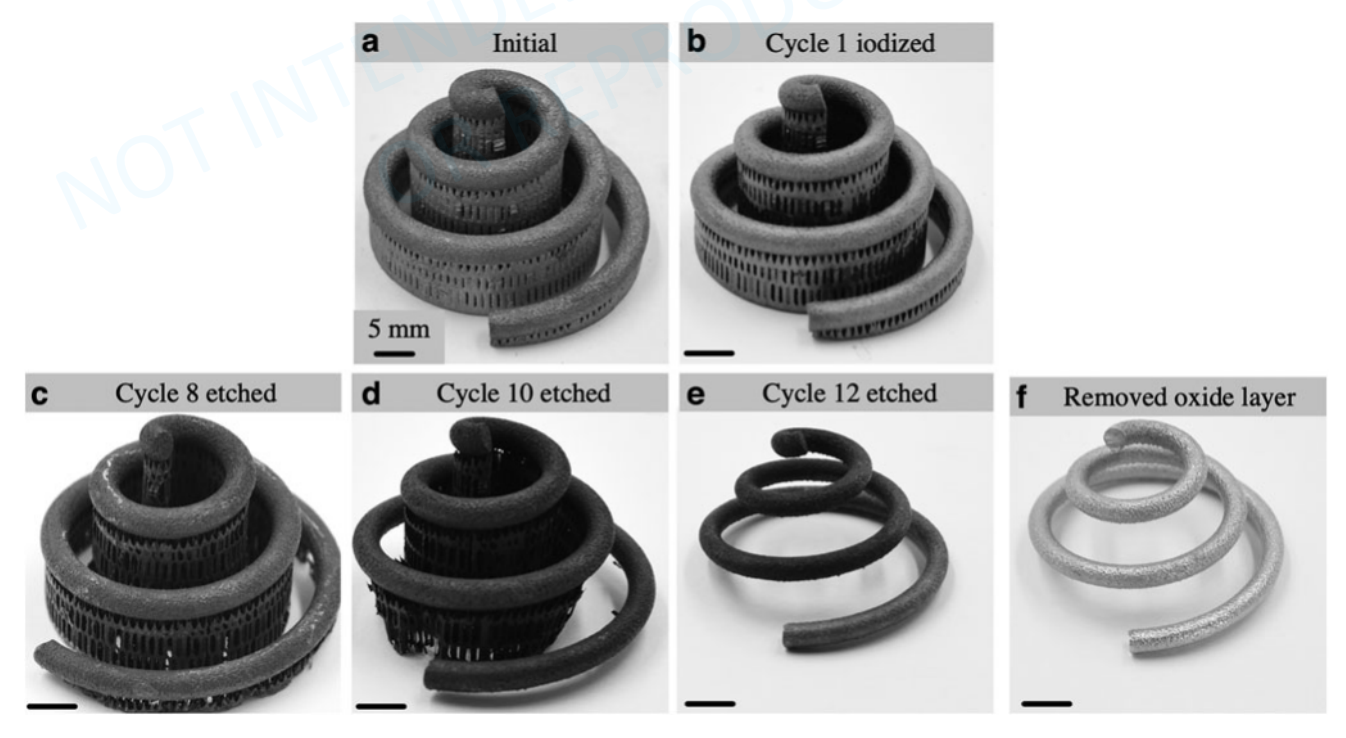


FIG. 8. Photos of HT-GRCop-42 spiral after different iodization—dissolution cycles. (a) Initial sample (as received), (b) 1 cycle iodization, after iodization—dissolution processes, (c) 8 cycles, (d) 10 cycles, (e) 12 cycles, and (f) after removing the trace surface oxides.

observed in optical microscopy images. The change of the thickness of the support in GRCop-42 after each cycle of iodization—dissolution was measured (Supplementary Fig. S8). A sharp decrease of the thickness of the support occurs in the first three cycles of iodization—dissolution and about 135 lm of GRCop is removed. In next three cycles, thickness change is not significant with the material losing about 56 lm. This decrease in the amount of material removed is attributed to low iodization penetration depth for these initial samples.

As a result, the open ends of the supports etched faster, and the supports were almost etched from the bottom-up instead of uniformly. Increasing the amount of iodine for the second set of samples (Fig. 9) improved penetration and reduced the number of iodization–etching cycles needed to remove the supports. It is worth noting that after six iodization–etching cycles, most of the support structures were dissolved (Supplementary Fig. S7c) so we were not able to do optical microscopy imaging and measure the thickness of the support after this stage.

To show the applicability of the self-terminating etching process on support removal in complex geometry of AM parts, we performed iodization and etching processes on both GRCop-42 and copper spirals and frogs (the photos of self-terminating etching process for frogs are shown in Supplementary Fig. S10). Figure 8 and Supplementary Figure S9 show the photos of HT-GRCop-42 and copper spiral samples after different iodization–etching processes, respectively. After 12 cycles, the whole support structure of 2 materials was dissolved.

The discoloration or darkening of the surface of both GRCop and copper is observed after each iodization—dissolution cycle because of the oxide particles remaining on the surface. Comparing Figure 8e and Supplementary Figure S9e shows that darkening in GRCop part is more than the copper part that can be due to the presence of Cr and Nb in GRCop and their reaction with oxygen. To remove the oxide particles from the parts, Wright's copper cream was used, and the clean surfaces of both HT-GRCop-42 and copper are shown in Figure 8f and Supplementary Figure S9f.

To clarify the amount of the material lost in self-terminating etching process, mass and diameter of the spirals were measured after different cycles (Supplementary Fig. S12). In general, the mass and diameter of both copper and HT-GRCop-42 spirals are reduced during self-terminating etching process. The change of the masses and radius of the samples is shown in the right axis of the plots. The material loss in both copper and HT-GRCop-42 spirals is almost same, and the total mass change in copper is 18.7 g and in HT-GRCop-42 is 18 g after complete removal of the support. From the diameter measurement, the copper and HT-GRCop-42 loss are \*314 and \*3651m after 12 cycles of iodization—dissolution.

It is worth noting that the diameter changes in both copper and HT-GRCop samples are not uniform that can be due to the inconsistency of the measurements after each cycle of self-terminating etching process. We also measured the change of the thickness of the support in different locations of spirals from optical microscopy images (Supplementary Fig. S11). The results indicate that same amount of material is removed from both copper and HT-GRCop-42 spirals after

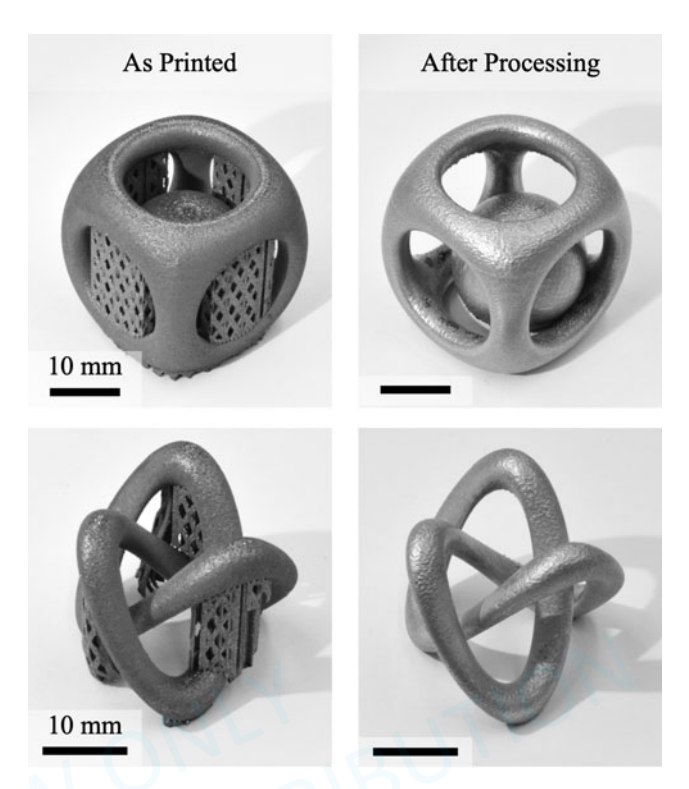


FIG. 9. Photos of GRCop parts before and after processing with higher iodine concentrations and shorter iodization (1–4h) and etching times (5 min sonication in H<sub>2</sub>O plus 5 min sonication in acetonitrile). While the sensitization and etching process still needs some optimization, the initial results show that the process has the potential to be reasonably fast.

eight cycles of iodization-dissolution, copper and HT-GRCop-42 (148 and 147 lm, respectively).

The initial support removal recipes were chosen arbitrarily to ensure that the supports were fully sensitized and dissolved because we only had those two samples. Additional samples arrived later, and we were able to test different sensitization and etching conditions to explore how much the process could be accelerated. The trapped sphere and Mobius shapes in Figure 9 were sensitized first for 1 h per cycle with relatively minor changes to the support structure observed. However, increasing the sensitization time to 4 h and the amount of iodine in the jar allowed us to fully remove the supports in about six cycles.

The etching time was also reduced by first sonicating in water for 5 min to remove most of the loosely adhered halide salt, followed by 5-min sonication in acetonitrile to fully dissolve the halide salts. This also resulted in a cleaner surface as judged by how shiny and bright the surface appeared. Overall, the process could be performed over a couple workdays instead of a couple weeks as with our first samples (the frog and the spiral). Future work will focus on quantifying the sensitization and dissolution kinetics so that processing parameters could be intelligently designed.

# Conclusions

In conclusion, we presented support removal in copper alloy (GRCop) components printed using SLM AM techniques

using self-terminating etching process. We introduced iodine as a sensitizing agent to alter the chemical composition of the top surface of GRCop and form a soluble iodide salt. We systematically studied the effect of iodization temperature and time on the resultant iodide layer and showed that iodization temperature has a more significant effect on the thickness of the iodide layer. Based on the EDS analysis, two layers are formed after iodization, which are composed of CuI outer layer along with a Cr- and Nb-rich iodide and oxide inner layer near the component surface. The oxide layer can be avoided by iodizing the component in an oxygen-free environment.

Treating the iodized GRCop with acetonitrile dissolves the iodide layers. Our results suggest that the removal of inner layer is a function of the sonication time, and it is completely dissolved after 30 min sonication. We also showed the effect of self-terminating etching method on the surface roughness of GRCop alloy. After four iodization-etching cycles, the surface roughness of GRCop-84 disks is reduced by about 70%. Overall, the utilization of the self-terminating etching process using iodine as the sensitizing agent is desirable for facile removal of internal and external supports, removal of any trapped powder, and the smoothing of interior and exterior surfaces in copper alloys. However, further studies are required to optimize the iodization process for obtaining thicker CuI layer (100-200 lm) that can result in more removal of the material and minimize the number of iodization-dissolution cycle.

#### Acknowledgments

We gratefully acknowledge the support from the Air Force Research Laboratory, the National Science Foundation, and the Colorado Office of Economic Development and International Trade. Any opinions, findings, and conclusions or recommendations expressed in this material are those of the author(s) and do not necessarily reflect those of the Air Force Research Laboratory, the National Science Foundation, or the Colorado Office of Economic Development and International Trade.

#### Author Disclosure Statement

No competing financial interests exist. The Authors are listed as co-inventors on United States Patent Applications related to the iodization processes used in this work.

# **Funding Information**

This study was supported by the Air Force Research Laboratory under Education Partnership number 19-EPA-RQ-12 (publication clearance number AFRL-2021-3017), the National Science Foundation (CAREER 1944516), and the Colorado Office of Economic Development and International Trade (CTGG1 20-2072).

#### Supplementary Material

Supplementary Table S1 Supplementary Figure S1 Supplementary Figure S2 Supplementary Figure S3 Supplementary Figure S4 Supplementary Figure S5 Supplementary Figure S6 Supplementary Figure S7 Supplementary Figure S8 Supplementary Figure S9 Supplementary Figure S10 Supplementary Figure S11 Supplementary Figure S12

#### References

- 1. Karthikeyan J. Development of oxidation resistant coatings on GRCop-84 substrates by cold spray process. NASA/Cr 20007=214706. https://www.asbindustries.com/documents/cr-2007-214706.pdf (last accessed April 21, 2021).
- Gradl PR, Protz CS, Ellis DL, et al. Progress in additively manufactured copper-alloy GRCOP-84, GRCOP-42, and bimetallic combustion chambers for liquid rocket engines. Proc. Int. Astronaut. Congr IAC, 2019. https://ntrs.nasa.gov/ citations/20190033311 (last accessed April 21, 2021).
- Thomas-Ogbuji LU, Humphrey DL, Greenbauer-Seng L. Oxidation behavior of GRCop-84 (Cu-8Cr-4Nb) at intermediate and high temperatures. NASA/CR 2000=210369. https://ntrs.nasa.gov/api/citations/20050123582/downloads/20050123582.pdf (last accessed April 21, 2021).
- Ellis DL. GRCop-84: A high-temperature copper alloy for high-heat-flux applications. NASA/Tm 2005=213566. https:// ntrs.nasa.gov/api/citations/20050123582/downloads/2005 0123582.pdf (last accessed April 21, 2021).
- Seltzman AH, Wukitch SJ. RF losses in selective laser melted GRCop-84 copper waveguide for an additively manufactured lower hybrid current drive launcher. Fusion Eng Des 2020;159:111762.
- Atzeni E, Salmi A. Economics of additive manufacturing for end-usable metal parts. Int J Adv Manuf Technol 2012; 62:1147–1155.
- Huang SH, Liu P, Mokasdar A, et al. Additive manufacturing and its societal impact: A literature review. Int J Adv Manuf Technol 2013;67:1191–1203.
- Srinivas M, Babu BS. A critical review on recent research methodologies in additive manufacturing. Mater Today Proc 2017;4:9049–9059.
- Strano G, Hao L, Everson RM, et al. A new approach to the design and optimisation of support structures in additive manufacturing. Int J Adv Manuf Technol 2013;66:1247–1254.
- Nelaturi S, Behandish M, Mirzendehdel AM, et al. Automatic support removal for additive manufacturing post processing. Comput Aided Des 2019;115:135–146.
- 11. Leary M, Maconachie T, Sarker A, et al. Mechanical and thermal characterisation of AlSi10Mg SLM block support structures. Mater Des 2019;183:108138.
- 12. Mezzadri F, Bouriakov V, Qian X. Topology optimization of self-supporting support structures for additive manufacturing. Addit Manuf 2018;21:666–682.
- 13. Wei C, Chueh YH, Zhang X, et al. Easy-to-remove composite support material and procedure in additive manufacturing of metallic components using multiple material laser-based powder bed fusion. J Manuf Sci Eng Trans 2019;141:071002.
- Greitemeier D, Dalle Donne C, Syassen F, et al. Effect of surface roughness on fatigue performance of additive manufactured Ti-6Al-4V. Mater Sci Technol 2016;32: 629-634.

Downloaded by Mary Ann Liebert, Inc., publishers from www.liebertpub.com at 01/05/23. For personal use only.

- 15. Romei F, Grubišić AN, Gibbon D. Manufacturing of a high-temperature resistojet heat exchanger by selective laser melting. Acta Astronaut 2017;138:356–368.
- Li Z, Zhang Z, Shi J, et al. Prediction of surface roughness in extrusion-based additive manufacturing with machine learning. Robot Comput Integr Manuf 2019;57: 488–495.
- 17. Raikar S, Heilig M, Mamidanna A, et al. Self-terminating etching process for automated support removal and surface finishing of additively manufactured Ti-6Al-4V. Addit Manuf 2021;37:101694.
- 18. Lefky CS, Zucker B, Wright D, et al. Dissolvable supports in powder bed fusion-printed stainless steel. 3D Print Addit Manuf 2017;4:3–11.
- 19. Lefky C, Gallmeyer TG, Moorthy S, et al. Microstructure and corrosion properties of sensitized laser powder bed fusion printed Inconel 718 to dissolve support structures in a self-terminating manner. Addit Manuf 2019;27:526–532.

- Noor EA, Al-Moubaraki AH, Corrosion behavior of mild steel in hydrochloric acid solutions. Int J Electrochem Sci 2008;3:806–818.
- 21. Turpin T, Dulcy J, Gantois M. Carbon diffusion and phase transformations during gas carburizing of high-alloyed stainless steels: Experimental study and theoretical modeling. Metall Mater Trans A 2005;36:2751–2760.
- Townsend A, Senin N, Blunt L, et al. Surface texture metrology for metal additive manufacturing: A review. Precis Eng 2016;46:34–47.

Address correspondence to:
Owen J. Hildreth
Department of Mechanical Engineering
Colorado School of Mines
Golden, CO 80401
USA

E-mail: ohildreth@mines.edu